ACS APPLIED MATERIALS & INTERFACES

Research Article

www.acsami.org

Pore-Size Dependent Protein Adsorption and Protection from Proteolytic Hydrolysis in Tailored Mesoporous Silica Particles

Daniel M. Schlipf,[†] Stephen E. Rankin,[†] and Barbara L. Knutson*[,†]

Department of Chemical and Materials Engineering, University of Kentucky, 177 F. Paul Anderson Tower, Lexington, Kentucky 40506-0046, United States

Supporting Information

ABSTRACT: Protein adsorption and interactions with mesoporous silica are of interest for a broad range of applications including drug delivery, chemical synthesis, biosensors, and bioseparations. A major challenge in designing mesoporous silica supports for tailored protein interaction is the differentiation of protein interactions at the surface of the particle from interactions within the pore, important features when considering mesoporous silica as a protective support for active proteins. In this investigation, the location of Enhanced Green Fluorescent Proteins (EGFPs) adsorbed on tailored mesoporous silica particles is examined as a function of pore diameter using proteolytic hydrolysis to distinguish between accessible and inaccessible proteins. Pore size control is achieved by tuning the hydrothermal aging temperature (60−110 °C) during synthesis, where the synthesis results in 5−15 μm diameter spherical particles appropriate for imaging by confocal scanning laser microscopy (CSLM). In low pH environments, EGFP unfolds within pores and on the surface of particles, rendering it susceptible to proteolytic hydrolysis by the protease Pepsin A. Upon return to neutral pH, un-hydrolyzed EGFP regains its fluorescence and can be visualized within the mesoporous particles. The pore-size dependent loading and protection of EGFP (2.4 nm diameter × 4.2 nm) from proteolytic attack by Pepsin A (7.3 nm × 3.6 nm × 5.4 nm) is demonstrated by the retention of fluorescence in 7.3 nm pores. Larger-pored materials (> 9 nm) provide diminishing protection for EGFP, and the protection is greatly reduced with increasing pore size and pore size distribution breadth. Proteolytic hydrolysis is used to delineate the activity of pore-loaded versus surface-bound proteins and to establish that there is an optimal pore diameter for loading EGFP while protecting it from attack by a larger proteolytic enzyme.

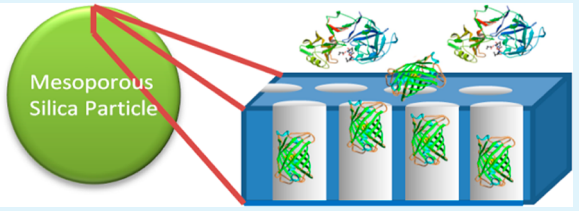

KEYWORDS: *mesoporous silica, protein adsorption, protein protection, size selective, proteolytic hydrolysis, fluorescent protein*

INTRODUCTION

Significant interest in the development of nano-scale protein encapsulation platforms has coincided with advances in the synthesis of mesoporous silica, which provide the ability to engineer nanoscale materials with fine control of the surface and pore environments. Mesoporous silica materials (MSMs) are inexpensive to produce, robust, and employ well known aqueous-based synthesis chemistry with existing applications as platforms for separations and catalysis.[1,2] The structures of MSMs can withstand high temperatures and pressures, are finely tunable, and synthetically versatile, allowing for a broad range of bulk forms (particles, monoliths, thin films), pore structures, and organic functional group incorporation. While the applications of MSMs for the separation and reaction of small molecules are well established, more recent interest in separations, catalysis, and controlled release using larger biomolecules has grown as advances in synthesis techniques have made pore diameters greater than 5 nm in spherical particles readily achievable.[3,4]

Approaches to increasing the pore diameters of MSMs for the encapsulation of proteins include the use of mixed cationic and non-ionic surfactant systems as well as aging the templated silica materials at increased temperatures before pore template removal.[5−12] Originally, Zhao et. al. reported the first large-pore mesoporous materials with well-ordered hexagonal close-packed pores having diameters as large as 30 nm.[13] These materials were denoted SBA-15 (Santa Barbara Amorphous batch 15). Initially developed using tri-block copolymer surfactants, such as Pluronic surfactant P123, these materials have significantly increased pore diameters as a function of synthesis temperature because of use of the large tri-block copolymers as the pore templating micelle.[7] Increasing the temperature of the micelles during particle formation incorporates more of the hydrophilic chain ends of the non-ionic triblock copolymer into the core of the micelle, thus increasing micelle size and subsequently pore diameter with increased aging temperatures.[7,13,14] The use of cationic surfactants such as CTAB as a cosurfactant along with P123 in acidic conditions yields spherical particles, with particle diameters dependent upon CTAB concentrations in solution.[7,12] Acidic conditions are used because of the lower rate of silica condensation at low pH, allowing the shape of the particle to assume a spherical shape to minimize surface area and surface free energy.[15] Large pore diameters capable of protein

Received: July 10, 2013
Accepted: September 24, 2013
Published: September 24, 2013

adsorption (> 6 nm) have been reported in micrometer-scale spherical P123-templated silica particles (5 μm−20 μm diameter) by adjusting the temperature during hydrothermal aging (from 80 °C to 125 °C).[4,7]

Because of the generally negative charge of silica materials and positive charge of most biological proteins at neutral pH, an inherent attraction is present between the surface of silica materials and proteins in solution.[16−18] The adsorption of proteins on the particle exterior and interior of pores provides different environments for the activity and stabilization of these adsorbates. The stabilization of proteins in biotechnology is dependent upon keeping the proteins active in an unnatural environment.[3] The confining effects of pore walls provide conformational stability to adsorbed proteins, thus protein encapsulation within the pores is desirable.[19] The ability to functionalize the exterior and interior of these structures extends their potential uses into biomimetic in vitro applications, using surface functional groups for drug delivery and targeted therapies.[20] Recently published reviews outline many of the applications of mesoporous silica as a biomaterial for encapsulating proteins as well as the potential for biological catalysis, size selective protein separations, biological signaling, and drug delivery.[3,16,17,21−23]

Several research groups have demonstrated the use of tailored pore diameters for size selective adsorption of proteins, concluding that large pore diameters increase the accessibility of interior surface area for protein adsorption.[5,6,11,24] Previously, protein depletion measurements in solution have been used to deduce protein loading on particles.[5,11] High resolution confocal scanning laser microscopy (CSLM) has recently been employed to visualize proteins throughout mesoporous silica particles.[6,9,10,25,26] The diffusion of fluorescently tagged proteins and biomolecules is easily imaged in the well-ordered hexagonal close packed columnar pore structures of MCM-41 and SBA-15 materials.[9,24,27] CSLM imaging has been used to demonstrate the diffusion resistance of enhanced green fluorescent proteins (EGFP) (2.4 nm × 4.2 nm) in the pore openings of random shaped (4.1 nm pores), rod shaped (2.9 nm pores), and spherical (5.5 nm pores) particles.[9] Size selective protein adsorption within large pored silica materials has been visualized using fluorescently tagged lysozyme and bovine serum albumin (BSA). Pores of 7.4 nm and 12.7 nm diameter are fully accessible to lysozyme (3.0 × 3.0 × 4.5 nm) while prohibiting diffusion of BSA (4.0 × 4.0 × 14.0 nm).[6] A pore diameter of 2.8 nm prohibited the diffusion of both lysozyme and BSA. Visualization studies have been complemented by computational studies of biomolecular diffusion, which suggest that significant diffusion resistance occurs in the boundary layer at the entrance to pores in which the pore diameter approaches the size of the proteins diffusing.[24]

Limiting active proteins to porous structures and confirming the location of proteins within the pores of the materials requires a technique to inactivate proteins that are located on the surface of the particles and not protected within pores. Proteases are common proteins that hydrolyze other proteins, rendering them inactive. EGFP, for example, is susceptible to proteolytic hydrolysis and inactivation by the porcine protease Pepsin A.[28] Hydrolysis of EGFP by Pepsin A results in a permanent loss of protein activity and fluorescence because of the preferential cleavage of peptide bonds between hydrophobic aromatic amino acids.[28] Nearly the entire protein sequence is required for chromophore formation, therefore cleavage of 1 of the 45 available hydrophobic aromatic amino acids provides inactivation of EGFP fluorescence.[28] The quantitative reproducibility of EGFP fluorescence inactivation by Pepsin A has led to its use in an assay to determine active Pepsin A concentrations.[28] The size of Pepsin A (7.3 nm × 3.6 nm × 5.4 nm) is slightly larger than that of EGFP (2.4 nm × 4.2 nm barrel), suggesting a range of pore diameters for size exclusion of Pepsin A, ensuring proteolytic hydrolysis of only surface bound proteins.[29] Pepsin A activity on SBA-15 mesoporous silica materials with 7.0 nm diameter pores is consistent with limited accessibility of larger substrates in the pores.[30] Small substrates (Z-L-glutamyl-L-tyrosine) demonstrated significantly increased Pepsin A activity compared to the larger hemoglobin, which showed diminished activity, suggesting steric hindrance of the protease.[30]

The inactivation of proteins located on the surface of the particle using proteases is a novel approach to examine the protective environment of proteins in porous materials as well as to achieve materials with only pore-loaded active proteins. The concept is demonstrated in this work for a fluorescent protein (EGFP)/protease (Pepsin A) system using pore-diameter tunable silica particles appropriate for CSLM. EGFP is used both as a probe to visualize protein position and as a functional protein that will become non-fluorescent upon degradation by Pepsin A. CSLM is used to investigate protein protection as a function of pore diameter based upon imaging both before and after exposure of fluorescent protein loaded particle to a proteolytic environment. EGFP loaded particles with pore diameters ranging from 5.4 nm−11.6 nm are exposed to a solution of Pepsin A at low pH, rendering EGFP susceptible to hydrolysis by active Pepsin A. The dimensions of EGFP, Pepsin A, and the pore diameter are used to interpret the results and to demonstrate size selective protein adsorption, protection, and localization within spherical mesoporous silica particles.

EXPERIMENTAL SECTION

Materials. EGFP (≥97%) were purchased from BioVision and were received in a 1 mg/mL solution of PBS. Acetone (≥99.5%), ACS certified HCl (12.1M), and citric acid (≥99.9%) were purchased from Fisher Scientific. Lyophilized Pepsin A (≥2,500 units per mg dry) was purchased from Worthington Biochemical. Tetraethyl orthosilicate (TEOS, ≥98%) and crystalline trichloroacetic acid (TCA, ≥99%) were purchased from Acros Organics. Cetyltrimethylammonium bromide (CTAB, 98%) was purchased from Research Organics. Two-hundred proof ethanol (ETOH, 200 proof) was purchased from Decon Labs. Pluronic P123 triblock copolymer ($(EO)_{20}(PO)_{70}(EO)_{20}$ where EO is an ethylene oxide unit and PO is a propylene oxide unit, MW_{avg}= 5800) was purchased from Sigma Aldrich. All materials were used as purchased, and dilutions were made using deionized, ultra filtered water purchased from Fisher Scientific.

Materials Synthesis. Spherical SBA-15 (SBAS) materials were prepared using an adapted version of Gartmann's synthesis procedure, as modified from the work of Katiyar.[6,27] Initially, 3.10 grams of P123 was heated in a round bottom flask in a 50 °C oven until melted. After this, 0.465 g of CTAB dissolved in 20 mL of deionized water was added to the P123. This solution was placed in a water bath at 30 °C and stirred vigorously while 7.8 mL of 200 proof ETOH and 45.9 mL of 1.5 M HCl were added. After the P123 completely dissolved, 10 mL of TEOS was slowly added drop wise. This solution was mixed for 2 h. At the end of 2 h, the solution was poured into a Parr 4748 Teflon lined bomb, which had been acclimated to the hydrothermal aging temperature, between 60 °C and 120 °C, prior to use. The sample was kept at the desired hydrothermal aging temperature in an oven for 3 days. At the end of the 3 day period, the sample was removed from the bomb and mixed in a high speed mixer to homogenize the solution.

After homogenization, the sample was filtered and rinsed with 50 mL of deionized water. After filtration, the sample was placed into a single walled Whatmann cellulose extraction thimble, and the surfactants were removed using Soxhlet extraction with 200 mL of acetone over 24 h. The extracted particles are designated as SBASx, where x is hydrothermal aging temperature in °C, which is the independent synthesis variable.

Particle Characterization. Pore diameter and surface area were measured from nitrogen adsorption experiments (Micromeritics Tristar 3000) conducted at 77 K. Samples were degassed at 120 °C for a minimum of 4 h under flowing nitrogen gas before analysis. Specific surface area was estimated using the Brunauer, Emmett, and Teller (BET) isotherm, and the pore diameter was estimated as the peak in the pore size distribution calculated by the method of Barrett, Joyner, and Halenda (BJH).[31−33] The particles were imaged using a Hitachi S-4300 Scanning Electron Microscope (SEM). SEM samples were prepared by sprinkling the particles onto double sided carbon tape and attached to 15 mm aluminum mounts with M4 threads. Excess silica materials were blown off of the sample with nitrogen. Samples were prepared 24 h in advance and left in a desiccator prior to being sputter coated in a gold−palladium alloy before analysis.

EGFP Fluorescence and pH-Based Denaturation and Renaturation in Aqueous Solution. The fluorescence of aqueous EGFP at room temperature was measured using a Varian Cary Eclipse fluorescence spectrophotometer. The "activity" of EGFP is interpreted from its fluorescence in the protein's folded state. Fluorescence experiments were performed at an excitation wavelength of 398 nm and excitation slit width of 5 nm, with the emission spectra measured at 508 nm. The stability of EGFP fluorescence was confirmed by monitoring its intensity in solution (11 μg/mL EGFP in 10 mM Tris-HCl at pH 7.5) in the absence of silica particles at room temperature for 30 h. After an initial decrease of fluorescence intensity of 20% over the first 2 h, the fluorescence intensity of EGFP remained constant. EGFP was denatured and renatured by pH using a combination of citric acid and Tris-HCl, as adapted from Malik et al.[28] Concentrated EGFP was diluted to 22 μg/mL in 10 mM Tris-HCl at pH 7.5. Upon use, 500 μL aliquots were denatured using 100 μL of 0.1 M citric acid solution to adjust the pH to 2.5. After 10 minutes, the fluorescence of the denatured sample was measured. The EGFP sample was renatured by returning the solution to pH 7.5 using 400 μL of 1M Tris-HCl at pH 8.5 and protein fluorescence while renaturing was monitored as a function of time.

Sample Preparation and CSLM Imaging of Protein-Adsorbed Silica Particles. All silica samples were pre-wetted before introduction of EGFP. Thirty milligrams of each SBAS material was first shaken with 1 mL of 10 mM Tris-HCl in a 1.5 mL centrifuge vial for 24 h. After 24 h these materials were centrifuged at 13,300 rpm for 3 minutes, and the supernatant was discarded. The wetted particles were re-dispersed in 0.5 mL of 22 μg/mL EGFP and shaken for 24 h to allow for EGFP diffusion into the particles. The silica particles were used to prepare three types of samples for CSLM: EGFP-adsorbed particles, pH-denatured/renatured EGFP particles, and pH denatured/Pepsin A exposed/pH renatured EGFP particles. Denaturation/renaturation of the protein adsorbed to the particles was performed by introducing 0.1 mL of 0.1 M citric acid to the protein loaded particles, reducing the pH to 2.5, and shaking for 10 minutes followed by raising the pH to 7.5 with the addition of 0.4 mL of 1 M Tris-HCl. Hydrolyzed EGFP-adsorbed particles were obtained by conducting the pH denaturation step, with shaking in the presence of 30 μg/mL Pepsin A in 0.1 M citric acid. The pH was raised in the same manner through the addition of 0.4 mL of 1 M Tris-HCl.

Samples of each type of EGFP/particle solution were prepared by dropping the suspended particles in EGFP solution onto glass slides and covering them with standard coverslips. The edges of the samples were sealed and samples were immediately imaged using a LEICA TSP SP5 Confocal Microscope. An argon laser was used to excite the fluorescent proteins over a 63X objective. The gain voltage on the photo multiplier tube detector was held between 995 and 1200 V. The scan speed was 400 frames per second. The CSLM images presented are slices through the center of a single particle or a pair of particles, where the scan corresponding to the approximate "center" of the spherical particles was established from greater than 20 scans of the spherical particles in the z-direction. Fluorescence intensity profiles were extracted by scanning along a line through the center of each particle in the CSLM images using ImageJ software (National Institutes of Health). Each set of images comparing the fluorescence of EGFP loaded into the particles at pH 7.5 and the subsequent image after exposing the same particles to Pepsin at pH 2.5 and increasing the pH back to 7.5 were obtained under the same microscope conditions.

RESULTS AND DISCUSSION

Spherical SBA-15 (SBAS) silica materials were chosen as the encapsulating structure for proteins based on their large particle size and sphericity, making them appropriate for imaging, as well as their large, tunable pore diameter range appropriate for protein loading. SEM images establish an average particle diameter range of 5 μm−15 μm for these spherical particles (Figure 1). As seen in Figure 1A, particles synthesized at 60 °C

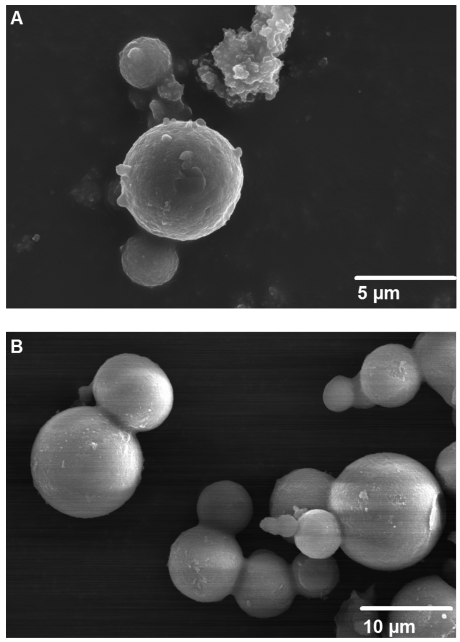

Figure 1. SEM images of SBAS materials synthesized at (A) 60 °C and (B) 120 °C.

are characterized by a rough particle surface. SBA-15 particles transition from "gyroid" to spherical morphology when synthesized between room temperature and 80 °C, therefore the rough surface of SBAS60, synthesized at 60 °C, could be attributed to this transitional structure (Figure 1A).[15] Materials synthesized at higher temperatures are smooth relative to materials synthesized at lower temperatures (for instance, SBAS120 in Figure 1B).

A key feature of these materials is the large, temperature-tunable pore diameter range appropriate for protein loading that can be achieved using the same surfactant template system (P123 and CTAB).[7] Increasing temperatures during hydrothermal aging increases the hydrophobic volume of the micelle templates, thus increasing micelle and template pore diameters.[7] The pore diameter of the synthesized materials, as determined by the BJH method, range from 5.4 nm to 11.6 nm over the range of hydrothermal aging temperatures (60−120 °C) (Table 1). All materials have type IV isotherms, which are

Table 1. Surface Area and Pore Diameter (Mode of the Pore Size Distribution) as a Function of Synthesis Temperature Determined by BET and BJH Methods, Respectively

sample	synthesis temperature (°C)	surface area (m^2/g)[a]	pore diameter (nm)[b]
SBAS60	60	819	5.4 ± 0.6
SBAS90	90	654	7.3 ± 1.5
SBAS100	100	532	9.2 ± 1.5
SBAS110	110	441	11.3 ± 1.2
SBAS120	120	311	11.6 ± 4.4

[a]The uncertainty of the surface area based on statistical analysis of the BET regression of a single measurement is less than ±2 m^2/g. [b]The reported range is the mode of the distribution ± the full width at half maximum

consistent with the well-defined mesoporous nature of these materials. The BJH pore diameter distribution for all synthesized materials is provided in Figure 2. Materials

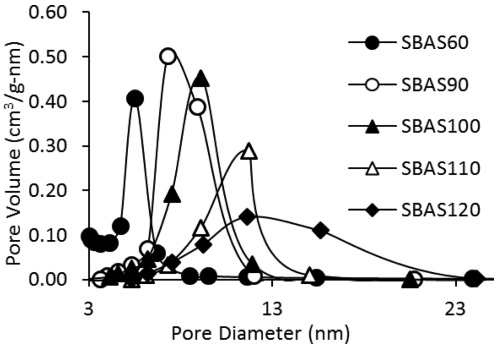

Figure 2. Effect of hydrothermal aging temperature on pore diameter distributions.

synthesized between 60 °C and 110 °C exhibit sharp pore diameter distributions, while a broader distribution is found at 120 °C. The presence of small mesopores is apparent in SBAS60 materials in Figure 2 and is due to the ethylene oxide units of the large P123 copolymer extending from the templating micelle and into the walls of the silica matrix.[7,13,14] At higher temperatures, these small mesopores disappear as the ethylene oxide units are incorporated into the hydrophobic core of the micelle.[4] The pore diameters could be tuned in a range spanning from a diameter near to the size of the protein to be encapsulated (EGFP 2.4 nm × 4.2 nm barrel, 26.9 KDa) to a diameter large enough to accommodate both the protein and the protease (Pepsin A, 7.3 nm × 3.6 nm × 5.4 nm, 34.6 KDa).[28,29,34,35]

The pore diameter of SBAS60 (5.4 nm) is slightly larger than the largest dimension of EGFP (4.2 nm) while the pore diameter of SBAS90 is the same as the largest dimension of Pepsin A (7.3 nm). The pore diameters of SBAS100, 110 and 120, 9.2 nm, 11.3 nm and 11.6 nm, respectively, are large enough for both the diffusion of EGFP and Pepsin A, potentially limiting the size selective protective abilities of the pores. Thus, this pore range is ideal to test the hypothesis that an optimal pore diameter exists that is adequate for loading and protection of only the target protein within the pores of these materials.

Enhanced green fluorescent protein (EGFP) was chosen for this protein encapsulation study because of its robust renaturing abilities during pH changes as well as its significantly greater stability over wild type GFP, minimizing the effect of time dependent protein unfolding over the period of the experiments.[28,36] Pepsin A is active below pH 4, a pH where EGFP is unfolded and non-fluorescent. In the presence of Pepsin A in acidic environments, EGFP undergoes proteolytic hydrolysis, rendering it incapable of refolding, thus permanently eliminating fluorescence.[28,36] Visualization of EGFP not hydrolyzed at low pH by Pepsin A requires an increase of pH back to pH 7.5, permitting recovery of fluorescence and subsequent visualization in CSLM. The hydrolysis of EGFP by protease Pepsin A at pH 2.5 and the ability of EGFP to regain fluorescence after exposure to pH 2.5 (in the absence of the protease) was confirmed in solution (Figure 3). In the absence

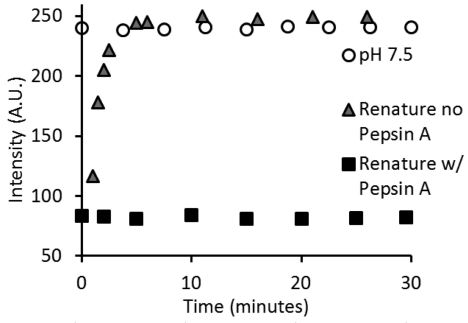

Figure 3. Fluorescence intensity of EGFP at pH 7.5, after denaturation at pH 2.5 and during renaturation at pH 7.5, and after exposure to Pepsin A at pH 2.5 and renaturing at pH 7.5.

of protease, full recovery of EGFP fluorescence is observed in going from pH 7.5 to pH 2.5 to pH 7.5. In contrast, a total loss of EGFP fluorescence is observed in an identical sample exposed to this denaturing and renaturing pH cycle in the presence of Pepsin A. The residual fluorescence intensity observed in the hydrolyzed protein solution is consistent with the background fluorescence from the solution.

CSLM was used to establish the location of fluorescently active EGFP in the 5 μm to 15 μm diameter silica particles. Figures 4 and 5 present the representative CSLM images and the corresponding fluorescence histograms taken across the center of a single spherical particle or pair of particles, respectively, as a function of the SBAS material. The first column in these figures is the fluorescence of the EGFP loaded particles prior to Pepsin A exposure. The second column is of the protein loaded particles after exposure to Pepsin A at pH 2.5 and renaturation at pH 7.5. The exception to the imaging of individual particles is the SBAS60 material (presented at 4× lower magnification). The particle clustering observable by CLSM is similar to SEM (Figure 1A), making this material less ideal for direct visualization of protein adsorption in pores. The histogram taken in Figure 5 is over one particle that was located within the cluster image of SBAS60 in Figure 4.

The CSLM images can be used to interpret the accessibility of the pores to EGFP and the size-dependent protection of the EGFP from proteolytic attack. Minimal diffusion of the protein into the smallest pore material synthesized (SBAS60, 5.4 nm pores) is observed, as indicated by a sharp ring of fluorescence intensity at the surface of the particles after exposure to EGFP for 24 h. The fluorescence of this surface bound protein is completely lost upon 10-minute exposure to Pepsin A, indicating that the standard protocol for EGFP hydrolysis by Pepsin A[28] is effective at hydrolyzing the surface protein.

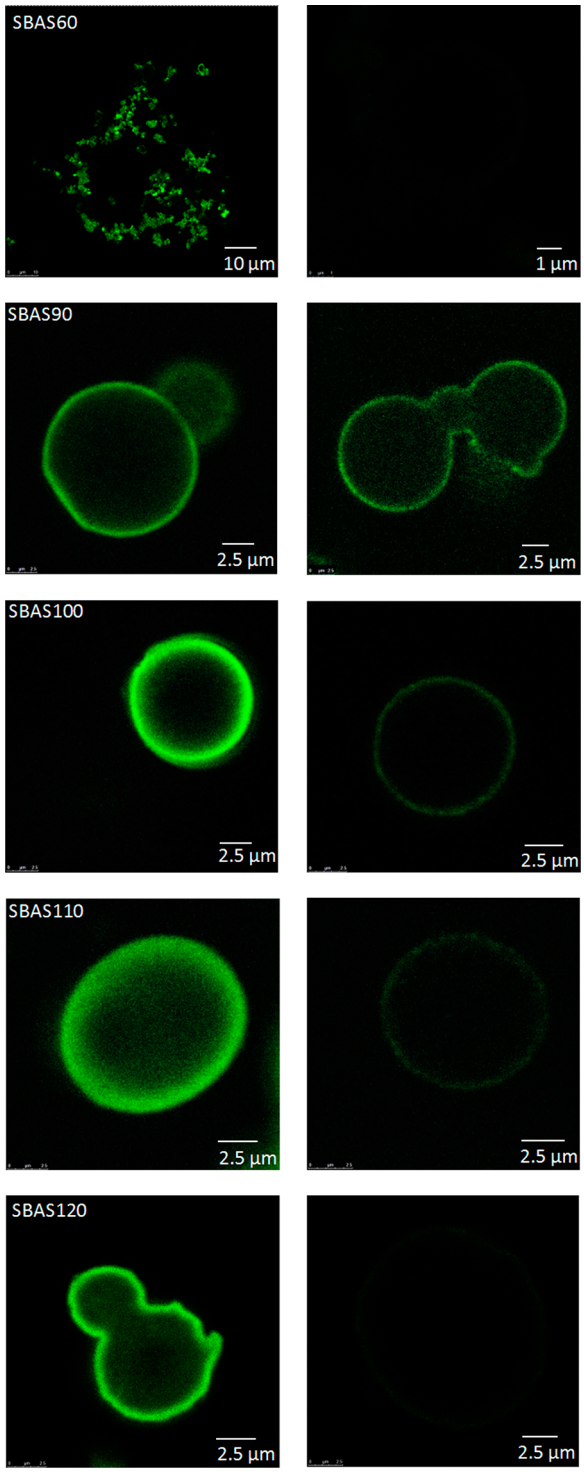

Figure 4. CSLM images of EGFP loaded mesoporous silica materials (column 1) and EGFP loaded materials after exposure to active protease (column 2). The contrast of SBAS90, SBAS100, and SBAS110 images were enhanced by .1% for the clarity. The contrast of SBAS60 and SBAS120 images were unmodified.

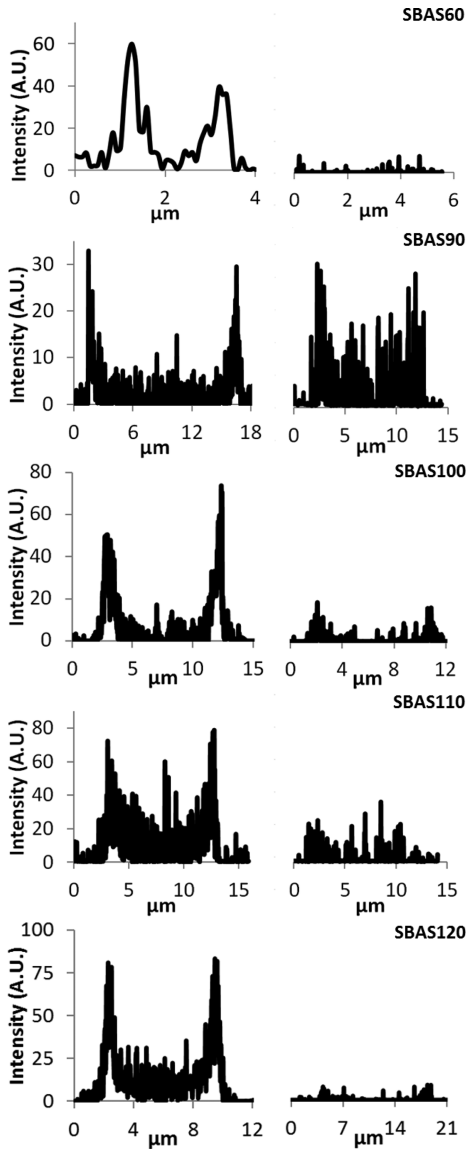

Figure 5. Histograms of the fluorescence intensity of EGFP loaded mesoporous silica materials (column 1) and EGFP loaded materials after exposure to active protease (column 2). Histograms correspond to images in Figure 4 without contrast enhancement, with the exception of the histogram for SBAS60 taken for a single particle from the cluster image in Figure 4. The source of the histograms from the original images is provided as Supporting Information.

Although the pore diameter is greater than the largest dimension of EGFP (2.4 nm × 4.2 nm), the pores of SBAS60 are too narrow for the diffusion of active EGFP molecules over a 24 h period. Protein accumulation on the surface of particles where protein dimensions approach the pore diameter has been attributed to the inability of native folded proteins to pass each other at the pore entrance.[24] While these images are similar to previous reports of GFP loading in porous silica,[9] our results uniquely establish the removal of surface proteins by proteases.

Increasing the pore diameter of the SBAS materials to 7.3 nm (synthesized with hydrothermal aging temperature at 90 °C) allows for significant EGFP loading within the pores as well as protection against proteolytic attack of the pore-loaded protein. Greater loading of EGFP within the pores is indicated by a more diffuse fluorescence intensity profile in the CSLM image that extends into the interior of the particles. Although the pore diameter is theoretically sufficient to permit diffusion of both EGFP (2.4 nm × 4.2 nm) and Pepsin A (7.3 nm × 3.6 nm × 5.4 nm), these pores provide the best protection against proteolysis (indicated by the highest level of fluorescence after Pepsin exposure relative to the intensity before exposure in

Figure 5). The accessibility of the protease to a pore of similar dimension may be hindered, as in the case of protein buildup of EGFP at the surface of materials with 5.4 nm pores. Alternatively, the pore diameter must also be sufficient to allow for access of the active site of the enzyme to the protein in its unfolded state, dimensions that are not predicted by protein size.

Higher hydrothermal treatment temperatures lead to larger pore diameters, 9.2 nm and 11.3 nm for SBAS100 and SBAS110, respectively. The pore diameters of these carriers allow for even more effective diffusion of EGFP, which leads to a greater fluorescence intensity throughout the entire cross section of the protein-loaded particles in Figures 4 and 5. However, the large pores of these materials also permit diffusion of Pepsin A into the pores and subsequent hydrolysis of EGFP. The decreased fluorescence of the EGFP after exposure to hydrolysis conditions is more pronounced for EGFP-loaded SBAS120, although the mode pore diameter of this material, 11.6 nm, is only 0.3 nm larger than SBAS110. Complete loss of fluorescence intensity throughout the spherical particles is observed after exposure to active Pepsin A at pH 2.5. The broad distribution of pore diameters in the SBAS120 material may contribute to its inability to protect EGFP towards proteolysis. Although 11.6 nm is the predominant pore diameter in this material, a significant fraction of pores of larger size (greater than 20 nm) is available for diffusion of EGFP and Pepsin A.

Protein protection from proteolytic hydrolysis would be overestimated and underestimated, respectively, if the pores of mesoporous silica materials provide conformational stability to encapsulated proteins,[17,19,23,37] suggesting that protein unfolding may be less favorable relative to bulk solutions. Our description of size selective protein adsorption and protection from proteases assumes that EGFP undergoes pH denaturation (unfolding) and renaturation (refolding) in mesoporous silica. In support of our described mechanism of size-selective protein protection, EGFP loaded SBAS90 was subjected to pH denaturation/renaturation in the absence of the protease. SBAS90 materials have the smallest pore diameter (7.3 nm) capable of significant EGFP loading in this study. The potential that the unfolding or refolding of EGFP is constrained by the pore size would be most evident in SBAS90 relative to the larger pore materials (SBAS100, SBAS110, and SBAS120). The fluorescence intensity histogram of EGFP within SBAS90 materials prior to lowering the solution pH (Figure 6A) and after denaturation at pH 2.5/renaturation at pH 7.5 (Figure 6B) are similar. The fluorescence of intermediate confocal images of EGFP loaded SBAS90 at pH 2.5 is indistinguishable from background noise, indicating denaturation of EGFP in the silica pores at low pH. The effective pH denaturation/renaturation of EGPF within silica pores is consistent with

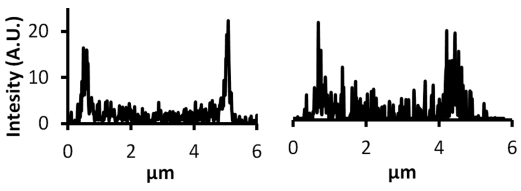

Figure 6. Histograms of the fluorescence intensity of EGFP loaded SBAS90, (a) at pH 7.5, and (b) after lowering to pH 2.5 and returning to pH 7.5 in the absence of a protease. The lack of EGFP fluorescence at pH 2.5 is not shown.

observations in silica gels that the difference in kinetics of unfolding are not distinguishable for GFPs confined in pores or in solution.[38] Stability of EGFP in SBAS90 is not due to confinement within the pores, but due to the pore diameter limiting the accessibility of Pepsin A to the unfolded EGFP.

CONCLUSION

This investigation provides direct evidence of size selective protein adsorption on porous spherical silica particles, a phenomenon that can be used to convey protective capabilities to pore loaded proteins or selectively remove proteins from particle surfaces using proteases. For the system of EGFP and Pepsin A, mesoporous silica with pore diameters greater than the diameter of the target protein provide for effective diffusion of the protein into the pores, while preventing rapid proteolytic attack within the pores even for a protease similar in size to the protein loaded in the pore. As the pore diameter increases beyond this optimal diameter, the loading of the target protein increases, but diffusion of the protease into the pores also increases, with the subsequent hydrolysis of the target protein. Increasing the synthesis temperature of SBAS materials increases the pore diameter, and also increases the pore size distribution at the highest synthesis temperature. Materials with a broad pore size distribution (SBAS120) provide significantly less protection of the target protein from hydrolytic attack, although the mode pore diameter of 11.6 nm represents only a slight increase in pore size relative to materials synthesized at a lower temperature (SBAS110, 11.3 nm).

The direct visualization of size selective protein protection and localization in porous materials made use of spherical SBAS materials, which were specifically chosen for this purpose based on their morphological homogeneity, narrow pore diameter distribution, and most importantly, particle size, allowing them to be imaged using CSLM. The use of EGFP, which is stable, robust to pH changes, and the use of Pepsin A to hydrolyze EGFP not protected within the pores were also critical to this investigation. However, the interpretation of size selectively and protein protection against hydrolysis is applicable to mesoporous materials in general. Our results show that, consistent with some of the earliest studies of protein loading into mesoporous silica, merely having a pore size slightly larger than or similar in size to the protein being adsorbed is not always adequate for protein loading.[5] The use of a protease allowed us to more clearly demonstrate that the protein is indeed loaded into the pore, and that co-diffusion of proteins follows a similar trend to single protein diffusion, namely, that the pore diameter must be larger than the combined diameters of the pair of proteins to permit significant entry of the larger protein to occur. Thus, when tuning mesoporous materials for protein loading and delivery applications, the optimal pore size for loading with protection is likely to be found between the diameter of the target protein and the sum of the diameters of the target protein and the smallest proteolytic enzyme able to attack that protein. Also, when co-diffusion of proteins is desirable (for example, when co-locating enzymes for sequential reactions in mesopores), the optimal pore diameter for protein loading is likely to be larger than the sum of the diameters of the two proteins. These findings demonstrate the value of techniques that provide complementary information to bulk adsorption, release, and activity measurements, namely, tuned micrometer-scale particles for visualization of protein location, and introduction of proteolytic enzymes for removal of surface-bound protein from the particle surface and confirmation of

protein protection. These techniques are suggested to be broadly applicable in the design of mesoporous protein nanocarriers.

■ ASSOCIATED CONTENT

Supporting Information

The supporting information includes the original CSLM images of the EGFP loaded and EGFP loaded Pepsin A exposed SBAS materials. These images indicate the scanning region from which the histograms in Figure 5 have been taken. This material is available free of charge via the Internet at http://pubs.acs.org.

■ AUTHOR INFORMATION

Corresponding Author

*E-mail: bknut2@uky.edu. Phone: 859-257-5715. Fax: 859-323-1929.

Author Contributions

The manuscript was written through contributions of all authors. All authors have given approval to the final version of the manuscript.

Author Contributions

†These authors contributed equally.

Notes

The authors declare no competing financial interest.

■ ACKNOWLEDGMENTS

This manuscript is based on work funded by the National Science Foundation Integrated Graduate Education and Research Training program on Bioactive Interfaces and Devices (Grant DGE-0653710). The authors thank Jim Begley of the University of Kentucky Imaging Facility for help with the CSLM experiments.

■ REFERENCES

(1) Kumar, P.; Guliants, V. V. *Microporous Mesoporous Mater.* **2010**, *132*, 1−14.
(2) Martín-Aranda, R.; Čejka, J. *Top. Catal.* **2010**, *53*, 141−153.
(3) Hudson, S.; Cooney, J.; Magner, E. *Angew. Chem., Int. Ed.* **2008**, *47*, 8582−8594.
(4) Katiyar, A.; Yadav, S.; Smirniotis, P. G.; Pinto, N. G. *J. Chromatogr. A* **2006**, *1122*, 13−20.
(5) Katiyar, A.; Ji, L.; Smirniotis, P.; Pinto, N. G. *J. Chromatogr. A* **2005**, *1069*, 119−126.
(6) Katiyar, A.; Pinto, N. G. *Small* **2006**, *2*, 644−648.
(7) Mesa, M.; Sierra, L.; López, B.; Ramirez, A.; Guth, J.-L. *Solid State Sci.* **2003**, *5*, 1303−1308.
(8) Ambati, J.; Lopez, A. M.; Cochran, D.; Wattamwar, P.; Bean, K.; Dziubla, T. D.; Rankin, S. E. *Acta Biomater.* **2012**, *8*, 2096−2103.
(9) Ma, Y.; Rajendran, P.; Blum, C.; Cesa, Y.; Gartmann, N.; Brühwiler, D.; Subramaniam, V. *J. Colloid Interface Sci.* **2011**, *356*, 123−130.
(10) Suh, C. W.; Kim, M. Y.; Choo, J. B.; Kim, J. K.; Kim, H. K.; Lee, E. K. *J. Biotechnol.* **2004**, *112*, 267−277.
(11) Sun, Z. K.; Deng, Y. H.; Wei, J.; Gu, D.; Tu, B.; Zhao, D. Y. *Chem. Mater.* **2011**, *23*, 2176−2184.
(12) Zhao, D.; Sun, J.; Li, Q.; Stucky, G. D. *Chem. Mater.* **2000**, *12*, 275−279.
(13) Zhao, D.; Feng, J.; Huo, Q.; Melosh, N.; Fredrickson, G. H.; Chmelka, B. F.; Stucky, G. D. *Science* **1998**, *279*, 548−552.
(14) Lin, H.-P.; Kao, C.-P.; Mou, C.-Y.; Liu, S.-B. *J. Phys. Chem. B* **2000**, *104*, 7885−7894.
(15) Yang, H.; Vovk, G.; Coombs, N.; Sokolov, I.; A. Ozin, G. *J. Mater. Chem.* **1998**, *8*, 743−750.
(16) Lee, C.-H.; Lin, T.-S.; Mou, C.-Y. *Nano Today* **2009**, *4*, 165−179.
(17) Sotiropoulou, S.; Vamvakaki, V.; Chaniotakis, N. A. *Biosens. Bioelectron.* **2005**, *20*, 1674−1679.
(18) He, J.; Liu, Z.; Hai, C. *AlChE J.* **2008**, *54*, 2495−2506.
(19) Dordick, J.; Freeman, A. *Curr. Opin. Biotechnol.* **2006**, *17*, 559−561.
(20) Yang, P. P.; Gai, S. L.; Lin, J. *Chem. Soc. Rev.* **2012**, *41*, 3679−3698.
(21) Kim, J.; Grate, J. W.; Wang, P. *Chem. Eng. Sci.* **2006**, *61*, 1017−1026.
(22) Hartmann, M. *Chem. Mater.* **2005**, *17*, 4577−4593.
(23) Hartmann, M.; Jung, D. *J. Mater. Chem.* **2010**, *20*, 844−857.
(24) Lu, S.; Song, Z.; He, J. *J. Phys. Chem. B* **2011**, *115*, 7744−7750.
(25) Lu, S.; An, Z.; Li, J.; He, J. *J. Phys. Chem. B* **2011**, *115*, 13695−13700.
(26) Wang, Y.; Caruso, F. *Chem. Mater.* **2005**, *17*, 953−961.
(27) Gartmann, N.; Brühwiler, D. *Angew. Chem., Int. Ed.* **2009**, *48*, 6354−6356.
(28) Malik, A.; Rudolph, R.; Söhling, B. *Anal. Biochem.* **2005**, *340*, 252−258.
(29) Sielecki, A. R.; Fedorov, A. A.; Boodhoo, A.; Andreeva, N. S.; James, M. N. G. *J. Mol. Biol.* **1990**, *214*, 143−170.
(30) Manyar, H. G.; Gianotti, E.; Sakamoto, Y.; Terasaki, O.; Coluccia, S.; Tumbiolo, S. *J. Phys. Chem. C* **2008**, *112*, 18110−18116.
(31) Bhambhani, M. R.; Cutting, P. A.; Sing, K. S. W.; Turk, D. H. *J. Colloid Interface Sci.* **1972**, *38*, 109−117.
(32) Brunauer, S.; Emmett, P. H.; Teller, E. *J. Am. Chem. Soc.* **1938**, *60*, 309−319.
(33) Barrett, E. P.; Joyner, L. G.; Halenda, P. P. *J. Am. Chem. Soc.* **1951**, *73*, 373−380.
(34) Ormo, M.; Cubitt, A. B.; Kallio, K.; Gross, L. A.; Tsien, R. Y.; Remington, S. J. *Science* **1996**, *273*, 1392−1395.
(35) Yang, F.; Moss, L. G.; Phillips, G. N. *Nat. Biotechnol.* **1996**, *14*, 1246−1251.
(36) Ward, W. W.; Bokman, S. H. *Biochemistry* **1982**, *21*, 4535−4540.
(37) Eggers, D. K.; Valentine, J. S. *Protein Sci.* **2001**, *10*, 250−261.
(38) Campanini, B.; Bologna, S.; Cannone, F.; Chirico, G.; Mozzarelli, A.; Bettati, S. *Protein Sci.* **2005**, *14*, 1125−1133.